4-20-2010

Traveling and Stationary Intrinsic Localized Modes and Their Spatial Control in Electrical Lattices

Lars Q. English
Dickinson College

F. Palmero

A. J. Sievers

P. G. Kevrekidis

D. H. Barnak
Dickinson College

Recommended Citation

English, Lars Q., F. Palmero, A.J. Sievers, P.G. Kevrekidis, and D.H. Barnak. "Traveling and Stationary Intrinsic Localized Modes and Their Spatial Control in Electrical Lattices." *Physical Review E* 81, no. 4 (2010): e046605. https://journals.aps.org/pre/abstract/10.1103/PhysRevE.81.046605

Traveling and stationary intrinsic localized modes and their spatial control in electrical lattices

L. Q. English,[1] F. Palmero,[2] A. J. Sievers,[3] P. G. Kevrekidis,[4] and D. H. Barnak[1]

[1]*Deptartment of Physics and Astronomy, Dickinson College, Carlisle, Pennsylvania 17013, USA*
[2]*Departamento de Física Aplicada I, ETSI Informática, University of Sevilla, Avd. Reina Mercedes s/n, 41012 Sevilla, Spain*
[3]*Laboratory of Atomic and Solid State Physics, Cornell University, Ithaca, New York 14853, USA*
[4]*Department of Mathematics and Statistics, University of Massachusetts, Amherst, Massachusetts 01003-4515, USA*

This work focuses on the production of both stationary and traveling intrinsic localized modes (ILMs), also known as discrete breathers, in two closely related electrical lattices; we demonstrate experimentally that the interplay between these two ILM types can be utilized for the purpose of spatial control. We describe a novel mechanism that is responsible for the motion of driven ILMs in this system, and quantify this effect by modeling in some detail the electrical components comprising the lattice.

I. INTRODUCTION

Intrinsic localized modes (ILMs), also known as discrete breathers, have by now been observed in a diverse collection of physical systems [1]. The presence of nonlinearity and spatial discreteness have served as the fundamental ingredients shared by the different applications. To exemplify the diversity, these systems have ranged from solid-state crystals [2–5] to micromechanical devices [6], Josephson junction arrays [7–9] and photonic crystals [10]. Recently, some studies have attempted to go beyond the mere experimental identification or even production of localized energy in various lattices to its direct manipulation and experimental control [2,6,11–13], a subject which has also been of interest to numerous theoretical studies [14]. In many of these studies the focus has been on protocols designed to move ILMs from one lattice site to another, as well as to control the interaction between two such localized modes.

In this paper, we present a straightforward method of achieving substantial spatial control of ILMs in the same electrical lattice in which ILMs have been observed recently [17,18]. As we will show, the method utilizes an idiosyncrasy of this system: there exist two closely related versions of the electrical lattice which admit, respectively (and exclusively), traveling or stationary ILMs. We then demonstrate that by locally switching between these two variants of the lattice, it is possible to capture a traveling ILM at any chosen lattice site, as well as to release it (into a traveling state) from that site.

The observation that of the two closely related versions of the lattice only one supports traveling ILMs, is key to explaining the origins of ILM motion in this system. We outline the mechanism by which the ILM "propels itself" in this system—one that is different from those reported in the literature for other systems. As we will see, the relevant mechanism (when present) enforces traveling within the electrical lattice, as the breather creates its own causes for motion. To quantify the mechanism, we model the components comprising the lattice in some detail and compare the resulting numerical predictions to experimental results. Along these lines, we also explore experimentally the formation of traveling ILMs in some detail and compare and contrast the initial modulational instability and subsequent pattern selection process that unfolds in the respective damped-driven lattices.

Our presentation will be structured as follows. In Sec. II, we will present the experimental system and the modeling approach/understanding toward its fundamental building block (i.e., the single element of the lattice). Then in Sec. III, upon explaining the fundamental difference between the two lattices, we will explore experimentally their features, including the outcome of the modulational instability, the seeding, capture, and release of ILMs and how they can occur in this system. Finally, in Sec. IV, we will summarize our findings and present our conclusions, as well as some directions for future study.

II. EXPERIMENTAL SYSTEM AND UNIT CELL

A. Experimental lattice description

Figure 1 shows a schematic of the two electrical lattices under investigation. They are very similar—both are one-dimensional bi-inductance lattices which act as band-pass filters. In the actual experiment, the lattices consist of 32 nodes and are fashioned into rings (so as to implement periodic boundary conditions), with the two inductances being $L_1 = 680$ μH and $L_2 = 330$ μH. The only difference between
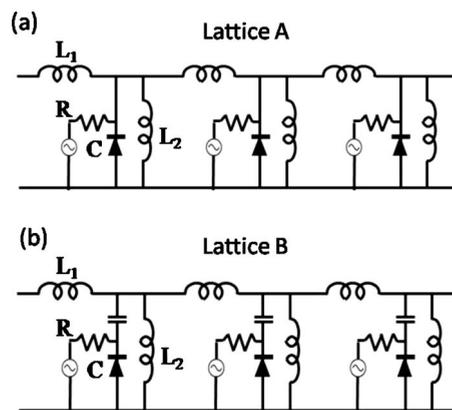

FIG. 1. The electrical lattice circuit (a) without and (b) with the blocking capacitors.

them are the additional capacitors which are present between the diodes and the inductor line in Fig. 1(b), whereas in Fig. 1(a) those capacitors are removed. The original purpose of this capacitor [15,16] was to block dc current from flowing through the resistor and inductor to the ground in the case where the driver contained a dc voltage offset. dc bias voltages were used in these previous studies for the purpose of biasing the diodes in order to vary their effective capacitance. The blocking capacitors then become necessary and their capacitance was chosen to be large so as not to modify the effective capacitance of the diodes themselves. In previous studies for instance [17,18], blocking capacitors of 1 μF were chosen, whereas the diodes had an effective capacitance of around 800 pF (at zero bias voltage)—i.e., a relative capacitance ratio of over a 1000. For this reason, one could naively surmise that the blocking capacitor would have no effect on the ensuing lattice dynamics.

As we will see, this expectation is only correct in the linear and weakly nonlinear regime, but does not hold in the fully nonlinear regime. When driven sinusoidally in time and homogeneously in space, lattice A (in Fig. 1) supports *only stationary* ILMs, whereas lattice B supports *only traveling* ones. Thus, we observe that when the blocking capacitors are removed from the lattice, the ILMs that are supported in the steady state by a continuous-wave driver spontaneously transform themselves from traveling to stationary ones. This will be the basis for our ability to controllably capture and release the ILMs in what follows.

B. Unit cell model, computation and comparison with experiments

In order to investigate the role of the blocking capacitor further, let us examine in detail a single unit cell of each electrical lattice. Figure 2(a) shows a schematic of the unit-cell circuit. The driver here is a sweep generator and the response of the circuit is measured by an oscilloscope at point A. The resulting frequency spectra are displayed in Figs. 2(b) and 2(c). In Fig. 2(b), the switch is set to position B such that the capacitor is by-passed, and in Fig. 2(c) the switch is set to position C such that the capacitor is included. The *x* axis displays frequency, and the *y* axis the most positive and negative voltage reached by an oscillation at that frequency. We see that in the linear and weakly nonlinear regime, the two responses are identical. However, as the driver amplitude is raised further, the spectra diverge significantly. The circuit without the capacitor exhibits an abrupt transition whose position depends on the direction of the frequency scan, as is characteristic of nonlinear oscillators. For clarity, only the down scans are displayed in the figure.

The circuit with the blocking capacitor exhibits a number of such transitions finely spaced within a certain frequency interval. The origin of these transitions is revealed by time profiles at isolated frequencies within this interval. We observe a periodic switching between a high-amplitude and a low-amplitude state at long periods on the order of 10 ms. The physical mechanism responsible for this low-frequency oscillation or switching will be identified in the next section; it is essential for the motion of ILMs in this system.
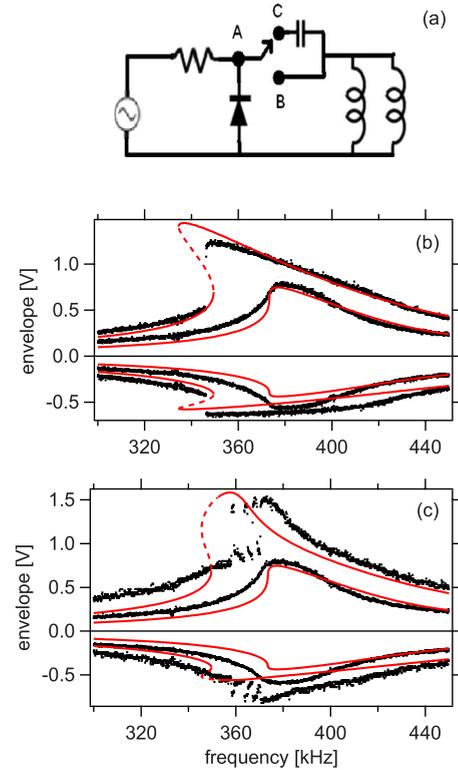

FIG. 2. (Color online) Testing the response of a unit cell at driver amplitude of 1 and 2 V. (a) Schematic of unit cell setup, (b) spectrum without, and (c) with the blocking capacitors. In Figs. 2(b) and 2(c), black points correspond to experimental data, continuous lines to stable solutions predicted by the theoretical model, and dashed lines to unstable solutions predicted by the theoretical model. In all cases $R = 10$ kΩ, $C_f = 1$ μF, $L_1 = 680$ μH, $L_2 = 330$ μH, $r = 16$ kΩ, and $C(0) = 832$ pF.

Figure 2 also depicts a theoretical prediction of the single-cell response which matches the experimental scans reasonably well. The asymmetry in the voltage envelope is seen in both the model and experiment and is a consequence of the current-voltage relationship of the diode (as will be explained below). Careful inspection of the theoretical curve reveals that in the case of $V_d = 2$ V and in the presence of the blocking capacitor, there exists an interval of frequencies where no solution (neither small nor large amplitude oscillation) is stable.

The main point (captured both by the experimental and numerical traces) is that the blocking capacitor does not alter the linear and weakly nonlinear properties of the lattice, but that it certainly does affect the strongly nonlinear regime in the dynamics.

Let us briefly outline the model used to describe the single-cell behavior. It is well known that diodes act as rectifiers, given by an asymmetrical current response of the kind,

$$I(t) = I_s(1 - Ae^{-\beta V(t)}). \tag{1}$$

Experimentally, it can be found in our setting that $I_s = 1.71 \times 10^{-11}$ A, $A = 2 \times 10^{-3}$, and $\beta = 37$ V^{-1}.

This current rectification is still operative into the radio-frequency regime, where the total current at the diode now also contains a capacitive contribution, $I = C(V)\frac{dV}{dt}$. It is evident that this contribution cannot give rise to a dc current offset, $I^{DC} = \frac{1}{T}\int_0^T I(t)dt$. In fact, we have experimentally verified that for radio frequency driving, I^{DC} through the diode (as measured via a small series resistor) is accounted for by Eq. (1). Thus, the correct model of the varactor diodes is an ideal diode [described by $I(V)$] in parallel with a nonlinear capacitor [described by $C(V)$].

If we consider that the driving source is given by $V_d = A\cos(\omega t)$, and using basic circuit equations, we can obtain a simple model for the unit cell without the blocking capacitor. This model is described by the equation:

$$C(V)\frac{d^2V}{dt^2} = -\frac{dI(V)}{dV}\frac{dV}{dt} - \frac{dC(V)}{dV}\left(\frac{dV}{dt}\right)^2 - \frac{(R+r)}{Rr}\frac{dV}{dt} - \frac{V}{L}$$
$$-\frac{A\omega}{R}\sin(\omega t), \qquad (2)$$

where V is the voltage across the diode. Here L is the effective inductance of the two inductors in parallel, and the parameter r represent the residual ohmic resistance of the circuit, the value of which must be high enough to render its effect small everywhere except near resonance. This resistance is necessary to reproduce the experimental spectra quantitatively and its value is on the order of 20 kΩ.

The equations for the unit cell with the blocking capacitor are slightly more complicated, as we have to distinguish between the voltage across the diode, V_D, and the voltage across the blocking capacitor, V_f

$$C(V)\frac{d^2V_D}{dt^2} = -\frac{dI(V_D)}{dV_D}\frac{dV_D}{dt} - \frac{dC(V_D)}{dV_D}\left(\frac{dV_D}{dt}\right)^2 - \frac{1}{R}\frac{dV_D}{dt}$$
$$+ C_f\frac{dV_f^2}{dt^2} - \frac{A\omega}{R}\sin(\omega t),$$

$$C_f\frac{d^2V_f}{dt^2} = -\frac{1}{L}(V_D + V_f) - \frac{1}{r}\left(\frac{dV_D}{dt} + \frac{dV_f}{dt}\right). \qquad (3)$$

The diode capacitance has been measured experimentally and can be reasonably approximated over the full range of voltages (-0.7 V $< V <$ 8.0 V) by the double-exponential fit

$$C(V) = C_0 + Ae^{-\alpha_1 V} + Be^{-\alpha_2 V}, \qquad (4)$$

where $C_0 = 21$ pF, $A = 652$ pF, $B = 27$ pF, $\alpha_1 = 0.34$ V^{-1}, and $\alpha_2 = 9.35$ V^{-1}. For positive voltages alone, a single exponential decay with amplitude of 810 pF and decay constant 0.53 V^{-1} is more accurate but fails for negative voltages (where the slope is much steeper).

III. FULL LATTICE RESULTS AND ANALYSIS

A. Static ILM distortions and the role of the blocking capacitor

Let us examine the voltages across and currents through the diode, first in the absence of the blocking capacitor (lattice A). The voltage across the diode, V_n, is the directly mea-
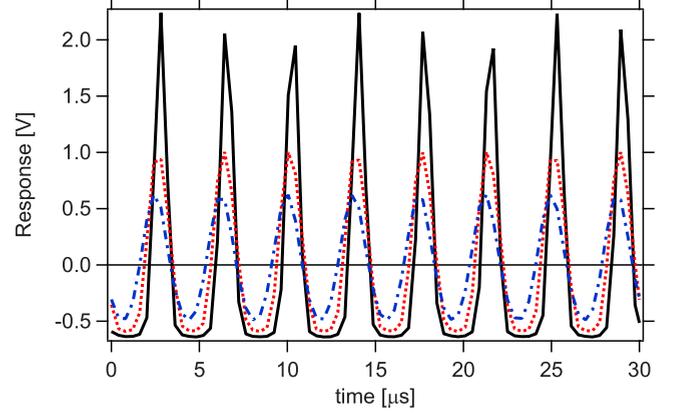

FIG. 3. (Color online) Voltage oscillation of the ILM center for a typical stationary ILM. The driver frequency and amplitude is 265 kHz and 3 V, respectively.

surable diagnostic in the experiment at a time resolution of 0.4 μs. This time-periodic voltage is far from sinusoidal at the ILM center (see Fig. 3), but its Fourier series must not contain a dc offset, as this would cause a very large current through inductor L_2. Thus, $V_n(t) = \Sigma_m A_m^{(n)}\sin(m\omega t)$.

In the experiment, we do not monitor the currents directly, but we can nevertheless estimate the magnitude of the ac currents, using the circuit equations

$$V_{n-1} - V_n = L_1 dJ_n/dt,$$

$$V_n = L_2 dK_n/dt, \qquad (5)$$

where J and K are the currents through inductors L_1 and L_2, respectively.

By numerical integration of Eq. (5) using the trace in Fig. 3, we find the peak to peak currents $J_{pp} = 2.0$ mA and $K_{pp} = 10$ mA at the ILM center. From the symmetry of the ILM voltage profile, it is evident that $J_n \cong -J_{n+1}$, and so currents from the three inductors connected to the ILM-center node n are all directed toward that node and (one half-cycle later) away from that node. By Kirchhoff's node rule, it is clear that this ac current has to be channeled through the diode.

At the diode, V_n causes a dc current according to Eq. (1). It is clear that this dc current flows in the forward direction, and it will be largest at the ILM center and rapidly decreasing to either side. We can estimate I_n^{DC} using V_n from Fig. 3 in conjunction with Eq. (1) and performing an integral over one period. This yields for the ILM center, $I_n^{DC} = 0.23$ mA, for the next site over, $I_{n-1}^{DC} = 0.023$ mA, and for the next-nearest neighbor, $I_{n-2}^{DC} = 0.32$ μA. The current does not strictly vanish in the wings due to the driver maintaining a certain voltage oscillation, but it becomes very small. These dc currents, I_n^{DC}, thus constitute a dc distortion in the lattice associated with the presence of the ILM.

In the case of lattice A, the dc currents (which are spatially concentrated at the ILM center) can easily flow to ground via the inductors L_2. In Lattice B, however, the blocking capacitors in series with the diodes prevent this flow of current to the ground. Instead, there the dc current charges up the blocking capacitor. The result is that the

blocking capacitor develops a dc voltage across it, with the positive side facing the diode, which in turn biases the diode and changes its effective capacitance.

Let us take a close look at the path of this dc current in the circuit. From a dc perspective, a number of points in the unit cell are grounded. The line containing inductor L_1 is at dc ground, and the left end of the resistor is held at ground by the function generator (see Fig. 1). The diode generates a dc current, I^{DC}, and is connected directly to ground at the bottom. Thus, we see that the capacitor can charge to a maximum voltage of $V_m = I^{DC}R$, and that the charging curve is characterized by a time-constant of $\tau = \frac{CV_m}{I^{DC}} = RC = 10$ ms. Based on the estimate of I^{DC} above, we calculate $V_m = 2.3$ V at the ILM center.

The end effect is that the ILM lowers the effective capacitance of the diodes and therefore raises the resonance frequency of the node at which it is centered. In essence, the ILM generates over time an impurity at its center site. The sign of this impurity is such as to repel the ILM from its center site [13]. For instance, if the capacitor were allowed to charge to its maximum voltage V_m, it would decrease the effective diode capacitance from about 810 to 237 pF. This, in turn, would cause a jump in local resonance frequency from $f = 265$ to 490 kHz, i.e., far into the linear dispersion curve. Once the ILM hops to the neighboring site (for times much faster than τ), the process repeats itself. Thus, we see that in lattice B, the ILM cannot linger, but is forced to move through the lattice because it continually creates the cause for its own motion.

This picture of ILM motion now readily explains two experimental observations. (1) The larger the ILM amplitude (or the stronger the ac driver), the larger the speed of the ILM through the lattice is, since the dc current is increased. (2) The larger the capacitance value of the blocking capacitor, the lower the speed of the ILM is, since it takes longer to generate the same voltage drop across the capacitor given the same dc current.

The effect of self-detuning due to the charging of the capacitor also occurs in the unit-cell setting of Sec. II, and this readily explains the aforementioned instability seen in the nonlinear-response spectra within certain frequency windows.

B. Modulational instability

One way to produce ILMs in both lattices is via the well-known modulational instability (MI) of the driven uniform mode. This has been used in mechanical [6], microwave [19] and optical systems [20] in order to produce such localized modes. Let us examine the MI route that leads to either stationary or traveling ILMs in detail.

Figure 4 compares the responses of the two lattices with and without the blocking capacitor to identical driving. As in all subsequent density plots, the gray shading represents energy (with darker shades corresponding to higher energies), and the time and space are plotted on the horizontal and vertical axes, respectively. Both lattices initially are unexcited before being subjected (at t=0 s) to a sinusoidal driver of 4.0 V amplitude and 290 kHz frequency. Comparing the
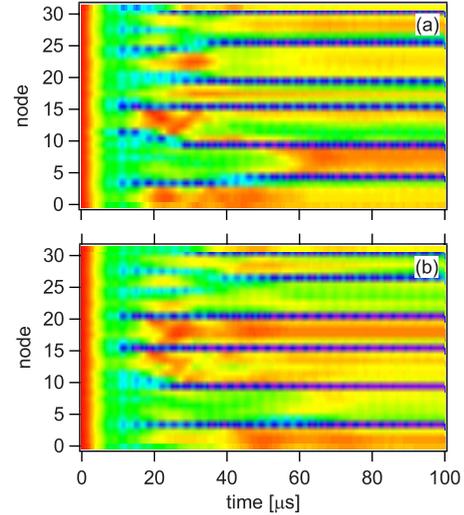

FIG. 4. (Color online) Experimental realization of the modulational instability of the driven uniform mode. Respectively, (a) and (b) indicate the lattices with and without the blocking capacitors. The space-time contour plots of the energy distribution over the lattice are shown in the panels.

two panels, it is apparent that the patterns induced by the modulational instability are almost indistinguishable. Both lattices exhibit an initial instability against the same spatial wavelength. This is consistent with the earlier finding for the unit-cell circuits where the blocking capacitor did not change the weakly nonlinear response. It is clear that the difference between traveling and stationary ILMs in this system cannot be traced to the initial modulational instability process that first creates localized structures as a result of the weakly nonlinear response of the system. It should instead be identified at the strongly nonlinear regime to be examined in more detail below.

Let us examine some further properties of the modulational instability in this system. Figure 5 shows the spatial voltage distribution at a series of time snapshots after the driver of 3.0 V amplitude is first turned on. The time slices were selected to display the maximum in each oscillation cycle. In Fig. 5(a), the driver frequency is 300 kHz, or just below the measured linear uniform mode frequency of 315 kHz. We see that at first the voltage and energy is uniformly distributed along the chain (solid trace at 11 μs). After 25 μs, a spatial modulation becomes apparent; the initial spatial wavelength of this modulation is fairly short, with six peaks appearing in the 32 node lattice (dashed trace at 42 μs). At longer times (dot-dashed trace at 120 μs), this wavelength increases somewhat (leading to a five-peak trace).

In Fig. 5(b), the frequency is lowered to 268 kHz. Here we observe that the spatial wavelength of the modulations increases significantly. The initial modulation is seen as fairly broad, containing only two peaks within the 32 nodes at $t = 20$ μs. This modulation eventually leads to only one ILM, shown at $t = 60$ μs, and eventually reaches its equilibrium amplitude after about 70 μs. It is evident that the eventual density of ILMs obtained in the lattice depends on the driver frequency, with lower frequencies resulting in lower
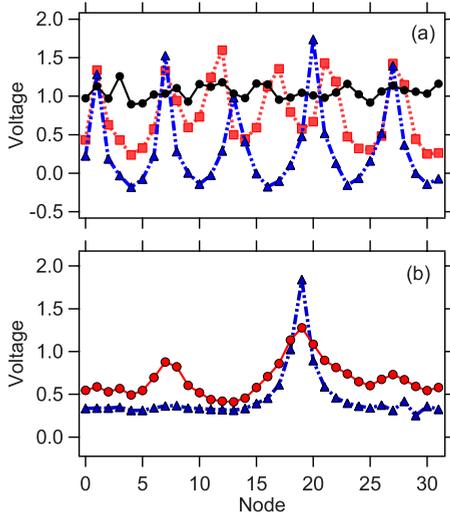
FIG. 5. (Color online) Snapshots at different times of the voltage dependence on the lattice node, illustrating the experimental manifestation of the modulational instability of the driven uniform mode for (a) 300 and (b) 268 kHz. The driver amplitude is 3 V. In the top panel, the solid line shows the lattice at 11 μs, the dotted at 25 μs and the dashed at 42 μs. In the bottom, we see the cases of 20 (solid) and 60 μs (dotted).

ILM densities. The connection is established via the details of the MI; when the driver is far below the uniform mode, the most unstable spatial wavelength is large, thus initiating fewer ILMs in the fully nonlinear regime at longer times.

Let us return to lattice B (with the blocking capacitors) to examine experimentally how traveling ILMs actually form. Figure 6 depicts a typical data set in that regard. Here the driver frequency and amplitude are set to 300 kHz and 5 V, respectively. At short times, the familiar modulational instability mechanism is observed as before. As the localized
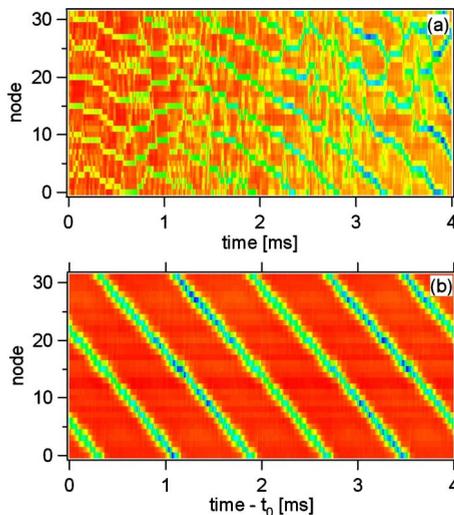

FIG. 6. (Color online) Similar to Fig. 4, but for a much longer evolution time scale. The modulational instability of the driven uniform mode is illustrated but also the path of self-organization toward a final state of two traveling ILMs is highlighted. (a) MI and pattern selection at short times and (b) at long times.

structures grow, a departure from the previous scenario occurs and the localized structures become mobile. In the figure, this happens after around 150 μs, and it is this development that is absent in lattice A. At this point, the mobile localized structures (six in number) start to organize themselves into patterns of motion. A sequence of processes ensues that results in fewer and more energetic ILMs; in the figure, this happens at around 1.25 ms and then again around 2.5 ms. Each time the number of localized structures is reduced but their strength increases; this type of scenario has been observed elsewhere as, e.g., in [21] (although there the resulting ILMs are stationary). Finally, only three traveling ILMs survive. Figure 6(b) shows the final situation obtained under continuous-wave driving conditions. (Note that the time axis starts at $t=t_0$, where t_0 is large compared to the interval shown.) Here a stable pattern of two traveling ILM is sustained as long as the driver is on. Further note that the speed of the localized features increases stepwise, as they consolidate and their amplitude gets larger. This result is consistent with Ref. [18] where the speed of the ILM was mapped as a function of driver amplitude and frequency. The difference is that here the ILM amplitude increases not due to changes in the driving conditions, but due to the self-organization process.

C. ILM seeding

Although MI is a particularly useful technique toward producing ILMs, one of its important disadvantages is that it relies on the manifestation of the instability, which naturally is a process whose exact dynamics is extremely sensitive to noise, and therefore in a perfectly periodic system the exact location of the pattern formed would be unpredictable, as would the eventual locations of the ensuing ILMs. In actual macroscopic lattices, such as this one, there will always be some small deviation from perfect periodicity due to the impossibility of manufacturing identical unit cells. These small lattice impurities will then guide the evolution of the MI into repeatable patterns that are nevertheless not controllable from the outset.

There is, however, a more direct alternative method toward the creation of ILMs in the electrical lattice [13]. The latter relies on creating a temporary impurity at a site chosen as the ILM center. Instead of using an actual impurity, however, in this section we demonstrate that switching locally between the two types of lattices discussed in this paper (with and without the blocking capacitor) can produce an ILM at a lattice site of our choice. In this scheme, a blocking capacitor is temporarily introduced at one particular lattice site (using an electronic switch) in a lattice otherwise free of such capacitors. Thus, the (integer) translational symmetry of the lattice is broken at one site. It is important to note that the introduction of the blocking capacitor does not change the linear (or weakly nonlinear) properties of the unit cell, however. In this sense, we do not introduce a linear impurity, but rather one that will only be activated in the highly nonlinear regime.

This switching action reproducibly results in the formation of an ILM, as shown in Fig. 7. Here, the onsite energy at
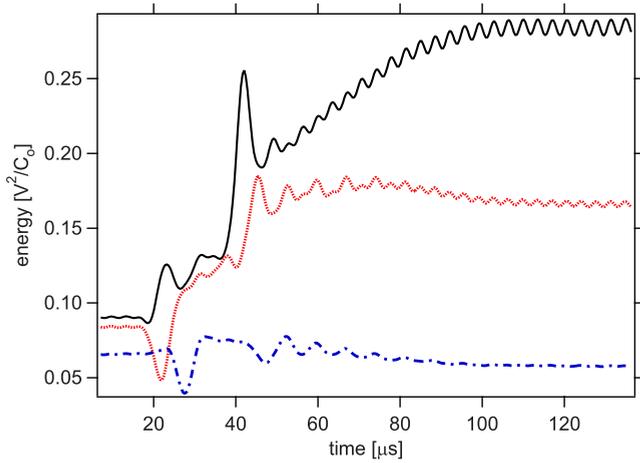
FIG. 7. (Color online) The energy evolution of three lattice sites (solid: ILM center, dotted: its nearest neighbor, dash-dotted: three sites away) as a blocking capacitor is switched on within a lattice of type A for 20 μs.

each node of the lattice is plotted versus time. It is calculated from the measured voltage via $E_n = 1/2C\langle V_n^2\rangle$, where the brackets indicate averaging over one period. Note that the switch turns on at 20 μs and off at 40 μs. The solid line depicts the energy evolution at the center of the ILM (the switch location), and the dotted and dash-dotted traces show N=1 (i.e., nearest neighbors) and N=3, respectively. The small oscillations in the solid trace are due to the actual voltage oscillations at 280 kHz (which persist due to imperfect box-car averaging).

We see that the edges of the pulse controlling the switch induce spikes in the response of the lattice node. The spike after the trailing edge of the pulse then imparts to the center site enough energy for it to be able to connect to the driver. The energy spike at the center site actually manifests itself after some time delay as a dip in energy at the neighboring sites. In cases where the pulse width is longer than the 20 μs, one can also observe the temporary creation of an "impurity" mode during the pulse (in quotes because the difference manifests only in the nonlinear regime). This impurity mode then merges with the ILM after the pulse ends.

It should be noted that additional ILMs can emerge spontaneously via MI if the driver frequency and amplitude are chosen appropriately. However, we find that there exists a fairly small region in parameter space, where MI is suppressed and a seeded ILM can still lock to the driver. For the data shown, we found that at a frequency of 280 kHz, the range in driver amplitude where both conditions are fulfilled is between 3.96 and 4.20 V. Below the lower bound, the seeded ILM cannot lock to the driver and dies out, whereas above the upper bound, additional ILMs are created via MI. The exact range does depend somewhat on the lattice site due to small variability of electronic components.

D. ILM capture and release

Finally, let us invert the situation of the previous section by starting with a lattice with the blocking capacitors in
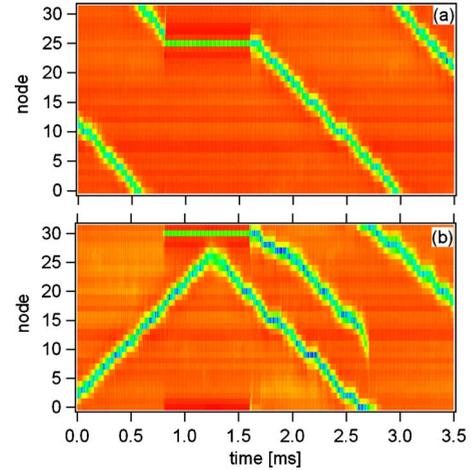

FIG. 8. (Color online) Two space-time evolution examples, upon turning on the nonlinear impurity (i.e., switching off the blocking capacitor) in a single node of an otherwise type A electric lattice. (a) The traveling mode gets captured and becomes a stationary mode at N=25 and is subsequently released (at will) by switching on the relevant capacitor anew. (b) Here the traveling mode collides with the stationary mode and is repelled from it. Subsequently, the blocking capacitor is turned on again, producing a moving ILM which eventually, however, fails to lock to the driver and disintegrates.

place (lattice B) and enabling one node to switch out this capacitor at particular times. Thus, we start with ILMs that travel through the lattice. The question is what happens when such a traveling ILM encounters a node without the blocking capacitor (i.e., the nonlinear impurity of such a node). Similar questions have been numerically monitored for ILMs in various settings, predominantly with linear defects [22,23], although examinations of nonlinear defects also exist [24]. Figure 8 illustrates what can result in this situation. The amplitude here is set to 4 V and the frequency to 280 kHz.

In Fig. 8(a), the capacitor is switched off (again using an analog switch controlled via a pulse generator) at the time the traveling ILM arrives at that node. In this case, the traveling mode gets captured and in effect becomes a stationary mode. Once the capacitor is reintroduced at the node, the ILM is released from the site and recovers its original speed.

In Fig. 8(b), the traveling ILM is not near the node at the time of the switching event and we see the traveling mode collide with the stationary mode (which is created by the switching event) at some later time. In this collision, the traveling mode does not merge but is clearly repelled from the stationary mode. In fact, the traveling ILM does not get any closer than about three lattice sites from the switched node before reversing its direction. In other instances, the traveling mode is repelled as well and attempts to reverse direction, but fails to lock to the driver and disintegrates very quickly.

While the interaction between the traveling breather and the impurity mode is always observed to be repulsive, this is not necessarily the case after the capacitor has been switched on anew, restoring the lattice periodicity. Now the traveling mode can merge with the breather at the former impurity site, before the latter has had time to depin from that site.
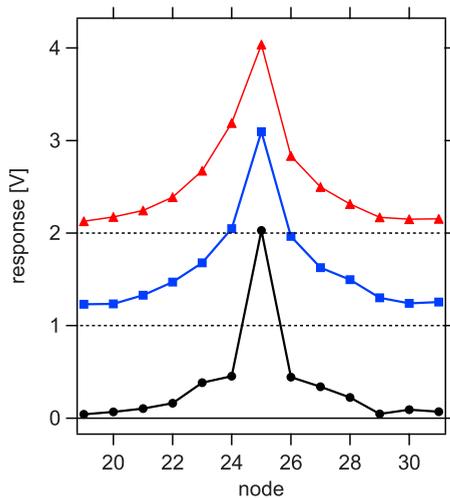
FIG. 9. (Color online) The ILM profile at various times. (a) Capacitor is switched off and the ILM is pinned, (b) 6.4 μs after capacitor is reinserted; the ILM is still stationary, and (c) ILM starts to move after 150 μs.

The main outcome of the above considerations is that when the timing of the switching event is chosen appropriately, the traveling ILM can be captured at a particular site indefinitely (a feature that has also been demonstrated theoretically/numerically in different settings [14]). It can also be released again by switching to the original configuration. In practice, the ILM is trapped at the leading edge of the pulse controlling the switch and released after the trailing edge. Interestingly, the stationary mode does not always immediately turn into a traveling ILM after the lattice periodicity is restored. In fact, it can take on the order of 100 μs for the ILM to resume its motion, during which time an asymmetry between the sites on either side of the ILM center gradually arises.

This is shown in Fig. 9 which depicts the ILM profile (driven at 278 kHz at 3 V amplitude) for various time slices. The lowest trace (circles) shows the localized mode during the time the capacitor is switched off. The second trace (squares) shows the ILM 6.4 μs (or almost two full oscillations) after the capacitor is switched back on. One difference is that the nearest neighbors to the ILM center have increased in amplitude. This is, in fact, the most noticeable change to the profile immediately after the capacitor is switched back on and lattice periodicity is restored. We see that a slight asymmetry (not present after the first oscillation) has already developed. This asymmetry continues to grow until the ILM actually hops to the neighboring site and begins traveling

through the lattice, as is illustrated in the uppermost trace (triangles) which shows the ILM profile after 150 μs. Comparing this time duration with results in Sec. III A, we find that a bias voltage increase (self-generated at the ILM center) of only about 35 mV, corresponding to a frequency shift of about 2.5 kHz, is sufficient to move the ILM to the neighboring site.

IV. CONCLUSIONS

The focus of this study has been twofold: first, to establish the mechanism responsible for ILM motion in the electrical lattice, and second, to demonstrate the experimental manipulation of ILM motion in an electrical lattice. Fast and accurate control of ILM motion has to be considered an essential prerequisite to future technological applications that may be derived from the phenomenon of energy self-localization. Here we have outlined a potential scheme for accomplishing such control in an electrical lattice.

In addition, we have uncovered a novel mechanism by which the ILM propels itself: mobility emerges as a result of the dc distortion associated with the ILM profile. Starting with a more complete understanding—through modeling/ simulation and their comparison with experiment—of the properties of the unit cell of these electrical lattices, we experimentally characterized in some detail the instabilities that lead to stationary and traveling ILMs in them. We thereby observed that the ILM motion is not imparted by the initial MI, but occurs subsequent to it, with the eventual pattern of traveling ILMs arising via a pattern selection process.

It would be of particular interest to try to generalize the modeling considerations herein to the lattice setting and try to obtain an analytical handle on the capture/release processes presented. Another relevant direction would be to generalize the considerations presented here to higher-dimensional settings and observe how traveling, capture, release and interaction phenomena are affected by the two-dimensional geometry. These aspects are presently under study and will be reported in future publications.

[1] S. Flach and C. R. Willis, Phys. Rep. **295**, 181 (1998); S. Flach and A. V. Gorbach, *ibid.* **467**, 1 (2008).
[2] J. P. Wrubel, M. Sato, and A. J. Sievers, Phys. Rev. Lett. **95**, 264101 (2005).
[3] M. E. Manley, A. J. Sievers, J. W. Lynn, S. A. Kiselev, N. I.

Agladze, Y. Chen, A. Llobet, and A. Alatas, Phys. Rev. B **79**, 134304 (2009).
[4] F. M. Russell and J. C. Eilbeck, EPL **78**, 10004 (2007).
[5] M. E. Manley, Acta Mater. **58**, 2925 (2010).
[6] M. Sato, B. E. Hubbard, and A. J. Sievers, Rev. Mod. Phys.

78, 137 (2006).

[7] M. Schuster, F. Pignatelli, and A. V. Ustinov, Phys. Rev. B **69**, 094507 (2004).

[8] A. V. Ustinov, Chaos **13**, 716 (2003).

[9] J. J. Mazo and T. P. Orlando, Chaos **13**, 733 (2003).

[10] F. Lederer, G. I. Stegeman, P. N. Christodoulides *et al.*, Phys. Rep. **463**, 1 (2008).

[11] M. Kimura and T. Hikihara, Chaos **19**, 013138 (2009).

[12] J. Wiersig, S. Flach, and K. H. Ahn, Appl. Phys. Lett. **93**, 222110 (2008).

[13] M. Sato, S. Yasui, M. Kimura, T. Hikihara, and A. J. Sievers, EPL **80**, 30002 (2007).

[14] P. G. Kevrekidis, D. J. Frantzeskakis, R. Carretero-González, B. A. Malomed, G. Herring, and A. R. Bishop, Phys. Rev. A **71**, 023614 (2005); M. A. Porter, P. G. Kevrekidis, R. Carretero-González, and D. J. Frantzeskakis, Phys. Lett. A **352**, 210 (2006).

[15] P. Marquié, J. M. Bilbault, and M. Remoissenet, Phys. Rev. E **49**, 828 (1994).

[16] M. Remoissenet, *Waves Called Solitons*, 3rd ed. (Springer-Verlag, Berlin, 1999).

[17] R. Stearrett and L. Q. English, J. Phys. D **40**, 5394 (2007).

[18] L. Q. English, R. B. Thakur, and R. Stearrett, Phys. Rev. E **77**, 066601 (2008).

[19] L. Q. English, M. Sato, B. E. Hubbard, and A. J. Sievers, J. Appl. Phys. **89**, 6707 (2001).

[20] J. Meier, G. I. Stegeman, D. N. Christodoulides, Y. Silberberg, R. Morandotti, H. Yang, G. Salamo, M. Sorel, and J. S. Aitchison, Phys. Rev. Lett. **92**, 163902 (2004).

[21] I. Daumont, T. Dauxois, and M. Peyrard, Nonlinearity **10**, 617 (1997).

[22] S. A. Kiselev, S. R. Bickham, and A. J. Sievers, Phys. Rev. B **50**, 9135 (1994); M. Sato, B. E. Hubbard, A. J. Sievers, B. ILic, and H. G. Craighead, Europhys. Lett. **66**, 318 (2004); V. Hizhnyakov, A. Shelkan, M. Klopov, S. A. Kiselev, and A. J. Sievers, Phys. Rev. B **73**, 224302 (2006).

[23] F. Palmero, R. Carretero-González, J. Cuevas, P. G. Kevrekidis, and W. Królikowski, Phys. Rev. E **77**, 036614 (2008); J. Cuevas, F. Palmero, J. F. R. Archilla, and F. R. Romero, J. Phys. A **35**, 10519 (2002); J. Cuevas and P. G. Kevrekidis, Phys. Rev. E **69**, 056609 (2004).

[24] P. G. Kevrekidis, Yu. S. Kivshar, and A. S. Kovalev, Phys. Rev. E **67**, 046604 (2003).